Non-wetting of condensation-induced droplets on smooth monolayer suspended graphene with contact angle approaching 180 degrees

Non-wetting of condensation-induced droplets on smooth monolayer suspended graphene with contact angle approaching 180 degrees

Haidong Wang[1†], Daniel Orejon[2,3†], Dongxing Song[1], Xing Zhang[1] **, Glen McHale[2], Hiroshi Takamatsu[4], Yasuyuki Takata[2,3,4], Khellil Sefiane[2,3] *

[1]Department of Engineering Mechanics, Tsinghua University, Beijing, 100084, China

[2]School of Engineering, Institute for Multiscale Thermofluids, University of Edinburgh, Edinburgh, EH9 3FB, Scotland, UK

[3]International Institute for Carbon-Neutral Energy Research (WPI – I2CNER), Kyushu University, Fukuoka, 819-0395, Japan

[4]Department of Mechanical Engineering, Kyushu University, Fukuoka, 819-0395, Japan

[†]These author contributed equally to the work.
*Corresponding author. Email: ksefiane@ed.ac.uk
**Corresponding author. Email: x-zhang@tsinghua.edu.cn

Abstract:

Superhydrophobicity is usually achieved by a combination of chemical hydrophobicity and surface topography due to an inability to attain complete non-wetting on the smooth surface of existing materials. Here, we experimentally report large non-wetting of condensation-induced droplets with contact angles approaching 180° on a smooth surface of suspended monolayer of graphene. Such highly non-wetting droplets are found on suspended monolayer graphene open to the water vapour saturated environment on both sides. Simultaneous observations of droplets condensing on monolayer and multilayer supported and suspended graphene demonstrates that this non-wetting behaviour may be unique to suspended monolayer graphene. These results anticipate that interactions between liquid molecules across a suspended monolayer isolated from a bulk substrate may induce large non-wetting beyond that possible on smooth hydrophobic or atomically flat supported monolayer surfaces.

Keywords:

Large non-wetting, suspended graphene, charge transfer, suspended monolayers, wettability manipulation, double-well potential, adsorbed layers

Introduction

The wetting properties of solids control a wide range of processes from the self-cleaning of biological surfaces to the anti-icing and anti-fouling properties of surfaces, hence designing surfaces with desirable wettability and functionalized properties is paramount to many current industrial and everyday applications as well as developing technologies[1-3]. Chemistry is the fundamental design tool used to tailor the wettability of a surface from hydrophilic to hydrophobic with polymer materials, such as Teflon™ (polytetrafluoroethylene). The intrinsic water repellency of Teflon™ is amongst the highest known to science and is exemplified by a contact angle, θ, of ca. 120° observed when a small droplet of water partially beads up when deposited onto a flat smooth Teflon™ surface (**Figure 1a**)[4]. This has been an absolute and fundamental limit (and barrier) in water repellence for any smooth material to date. To address the desire to create complete non-wetting surfaces, the last few decades of research has focused on amplifying the intrinsic hydrophobicity of surfaces through topographic structuring to create superhydrophobicity *via* a bed-of-nails ("Lotus") effect[5-9], or generating a vapor layer between the substrate and the liquid ("Leidenfrost")[10,11].

The prevailing strategy to achieve super water repellency has been to replace the solid-liquid interface by increasing fractions of liquid-vapor interface. The presence of micro- and/or nano-structures has been an imperative requirement to confer a surface with superhydrophobic properties starting with contact angles for water and other fluids on smooth surfaces limited to 120° or less[12-15]. The principle of these surfaces is to manipulate surface structure and/or the intrinsic wettability of the outermost surface so that capillary penetration between surface features is unfavorable[8,14-16]. The droplet then bridges across tips of surface features and effectively sits on a composite of the solid and air (**Figure 1b**). In the simplest model for a droplet resting above the surface features in the Cassie-Baxter (CB) state, the cosine of the observed macroscopic contact angle, θ_{CB}, is a weighted average using the solid (S) surface fraction, φ_s, and the air fraction, $(1 - \varphi_s)$[16,17]. Thus, the contact angle approaches complete non-wetting when the solid surface fraction vanishes. Conceptually, when the length scale of surface features becomes vanishingly small a droplet supported entirely by air and a droplet surrounded by only air will adopt a completely spherical shape with $\theta_{CB} \rightarrow 180^o$, under the action of surface tension to minimize its surface free energy. Such an ideal situation is similarly observed when a droplet touches a very hot surface, which is above its Leidenfrost point[7,8] or at ambient temperature on a low pressure

environment[18,19] and an instantaneous vaporization of a layer of water occurs resulting in a beaded up spherical droplet resting on a layer of its own vapor (**Figure 1c**).

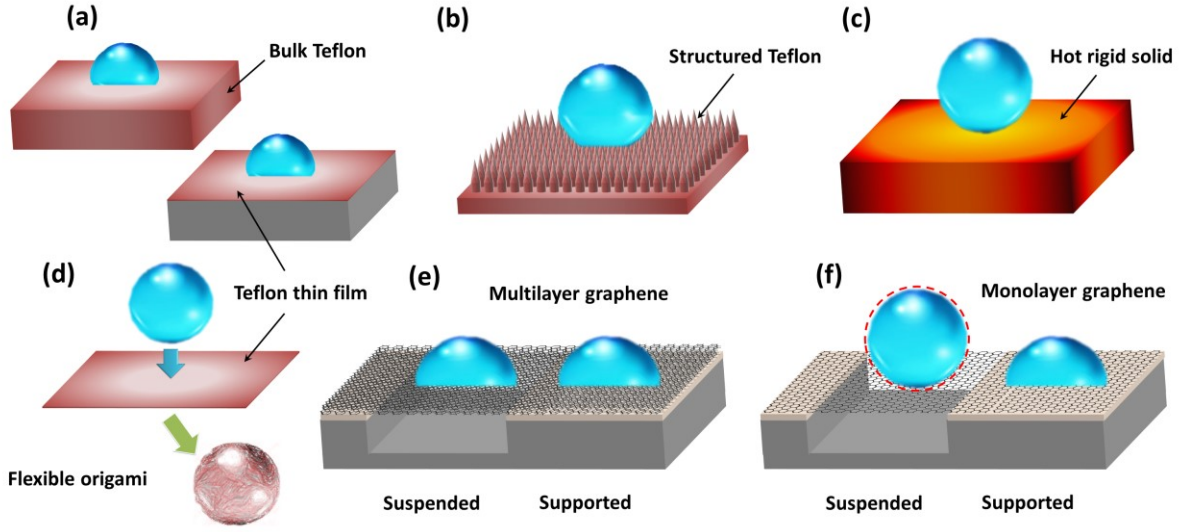

Figure 1 Schematic representation of wetting and non-wetting of liquids on various materials. **(a)** non-wetting on bulk rigid Teflon™ and on surface coated with a thin film of Teflon™, **(b)** non-wetting on superhydrophobic structured Teflon™ bed of nails, **(c)** non-wetting on a very hot rigid material, **(d)** wetting of hydrophobic Teflon™ thin film wrapping itself around the droplet as in Capillary Origami[20], **(e)** wetting on suspended and on supported multilayer graphene, and **(f)** wetting on supported monolayer graphene and non-wetting on suspended monolayer graphene where non-wetting droplet is highlighted by a red dashed circle.

Whilst the current strategy to achieve complete non-wetting is able to produce completely beaded up droplets, it does not address the fundamental question of how to achieve superhydrophobicity or non-wetting on a continuous and smooth solid surface. It does, however, highlight that a key issue is the interaction of the droplet with the solid substrate. In that regard, we anticipate that reducing the thickness of the substrate, t, to a size comparable or less than the interaction length scale between the liquid and solid may effectively remove the interaction with the substrate or surroundings with the consequent expected change from wetting to non-wetting behaviour approaching contact angles ca. 180°. However, for a membrane-like substrate its rigidity scales as t^3, and so it completely wraps itself around the liquid droplet even if the substrate is hydrophobic, such as Teflon™ (**Figure 1d**); this effect is known as Capillary Origami[20-22]. In view of the above, a strategy for exploring wetting and water repellency, beyond that possible on smooth hydrophobic substrates and without using topographic structuring, is to i) use a membrane of a material allowing for long range interactions beyond its thickness, and ii) suspend the membrane across a gap between two surfaces to avoid the occurrence of Capillary Origami.

To demonstrate this strategy, we therefore created mono and multilayers of graphene on a silicon substrate patterned with holes and trenches. The suspended monolayer graphene may have negligible interaction with water on top, known as the "wetting transparency" suggested in the literature[23-25]. We were able to create solid membranes of differing thicknesses (i.e. layers) either backed by silicon or bridging across gaps and so backed by its own vapor (or vacuum). By condensing droplets across the entirety of the surface it was then possible to investigate both the effects of membrane thickness and the solid (i.e. supported) *versus* vapor (or vacuum) backing of the membrane (i.e. suspended) on the observed wetting properties (**Figure 1e,f**).

Direct experimental observations of micrometer/picoliter droplets condensing on monolayer suspended graphene showed non-wetting droplets with contact angles as high as 175°, whereas wetting droplets with contact angles near or below 90° are reported on supported monolayer and on supported and suspended multiple layers graphene. Simultaneous observations on suspended and supported graphene for monolayer, two layers, four layers and multi-layer, statistical analysis, and additional considerations on pinning and sample quality demonstrate that non-wetting of water droplets on smooth monolayer with contact angles above those on Teflon™ may be possible by removing the water-surface interactions beyond the first surface layer in the case of graphene. Wettability manipulation through suspended graphene through control of the environment behind the suspended graphene layer suggest great potential for microfluidic applications and calls for the further investigations on other monolayer materials.

Results

Suspended Monolayer Graphene Characterisation

For our experimental observations we used monolayer (1L), 2 layers (2L) and 4 layers (4L) of graphene and multilayer graphite (ML) supported and suspended over holes and trenches. For simplicity, we henceforth refer to suspended graphene with the superscript ^{sus} and to supported graphene with the subscript $_{sup}$. Surface characterization of the fabricated 1L substrate is shown in **Figure 2**. More details and description of the surface fabrication and characterization for all fabricated and characterised substrates are given in within the Methods Section in sub-sections: Substrate Fabrication and Sample Characterization of 1L Suspended Graphene and within the accompanying Supplementary Note 1. Substrate Fabrication and Supplementary Note 2. Sample Characterization, respectively. More specifically **Figures S1, S2, S3 & S4** in the accompanying Supplementary Note 2.1 Sample Characterization by Optical Microscopy and SEM provide optical microscopy and Scanning Electron Microscopy (SEM) snapshots of both supported and suspended 1L, 2L, 4L and ML graphene, respectively. While **Figure S5 & S6** accompanying Supplementary Note 2.2 AFM Topography Characterization of Surface Roughness of Graphene show Atomic Force Microscopy (AFM) experimental observations on suspended and supported (over different types of substrates) 1L graphene and supported 2L, 4L and ML graphene, respectively.

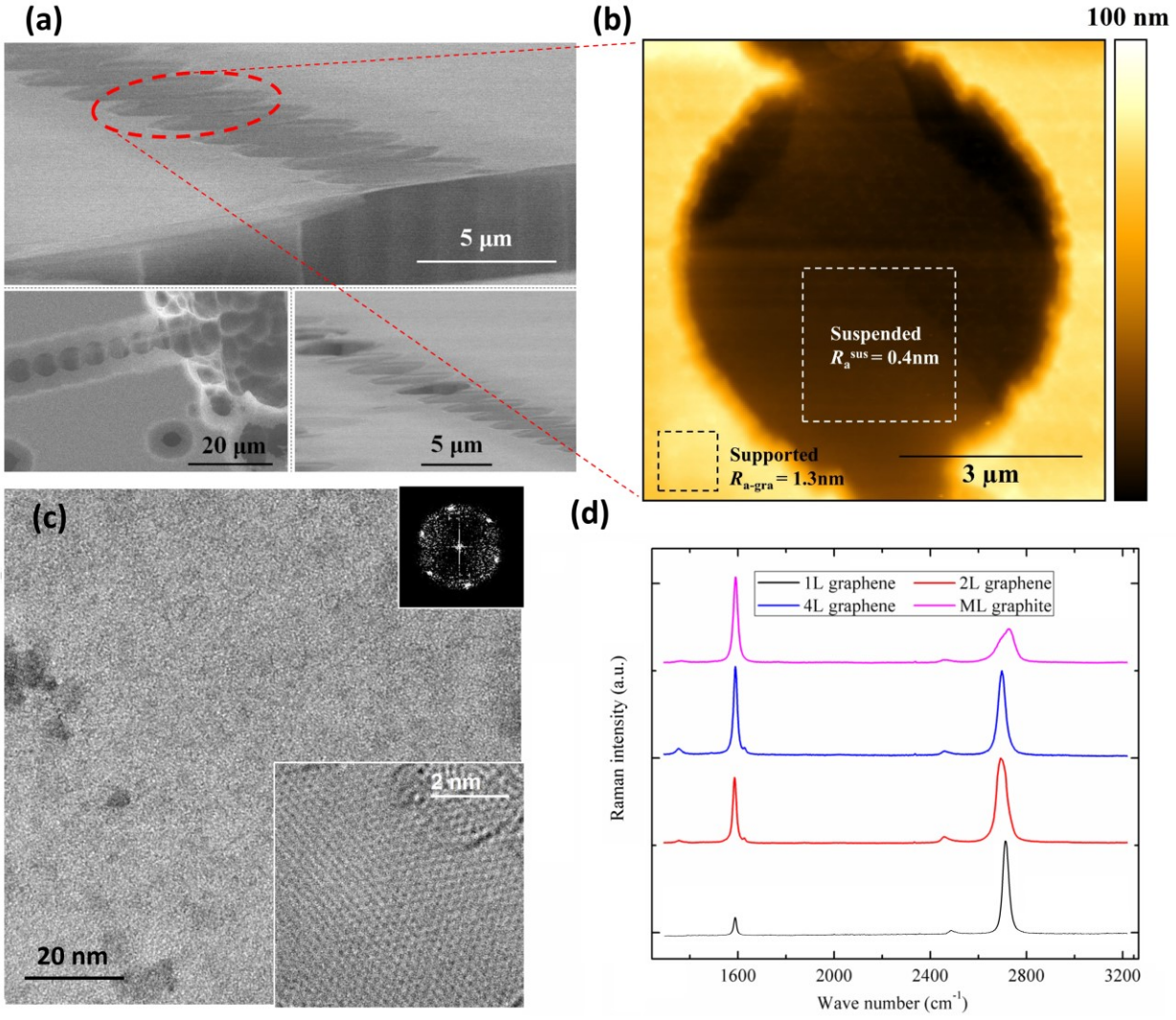

Figure 2 Surface characterization of 1L graphene. (a) Scanning Electron Microscopy (SEM), **(b)** Atomic Force Microscopy (AFM) height image of an area of 7.5×7.5 µm^2, **(c)** Tunnelling Electron Microscopy (TEM) and **(d)** Raman spectroscopy. **Figure 2b** also includes the root mean square surface roughness of suspended monolayer graphene, R_a^{sus} = 0.4 nm. Inset of **Figure 2c** bottom-right includes enlarged high-resolution TEM image and top-right shows Electron Diffraction (ED) pattern of 1L^{sus}. **Figure 2d** shows Raman spectra of 1L, 2L, 4L graphene and ML graphite, where the intensity ratio between 2D band (~2700 cm^{-1}) and G band (~1580 cm^{-1}) correlates to number of layers with an I2D/IG ratio of nearly 5 for 1L^{sus} in agreement with Ref. 34.

Condensation Experimental Characterisation

Direct contact angle measurements of sessile droplets on suspended graphene (1L^{sus}) are scarce to date as a consequence of the impossibility to create large suspended regions, by current fabrication and cleaning procedures, large enough to allow for macroscopic sessile droplet deposition or microgoniometry direct wettability measurements. Note that the minimum size of droplets generated via microgoniometry is at least one order of magnitude greater than the

fabricated area of $1L^{sus}$ [26]. Thus, to date, the wettability of graphene has been assessed exclusively by indirect methods such as measuring the contact angle of a bubble immersed in water in contact with monolayer graphene[27] or rolling a droplet of water over monolayer graphene powder[28]. Hereafter, to allow for the immediate and intimate visualization of the interactions between droplets with sizes in the order of micrometers in diameter or smaller (femtoliter droplets) and the different suspended and supported graphene substrates, we make use of the excellent spatial resolution provided by Environmental Scanning Electron Microscopy (ESEM) (FEI Versa 3D™, Hillsboro, Oregon, U.S.A.). We would like to note here that despite the excellent spatial resolution of ESEM, there are other shortcomings associated such as the impossibility of carrying out receding contact angle measurements of micrometre sized droplets and hence contact angle hysteresis characterisation.

Although most of the research work making use of ESEM reports on the qualitative interactions between condensing droplets and solid surfaces[29,30]; Zhang et al. recently reported, quantitatively, on the wettability of suspended monolayer graphene over a holey substrate atop a Tunnelling Electron Microscopy (TEM) grid, i.e., closed holes [31]. Here seemingly as in the work of Zhang et al., we provide further quantification on the contact angles adopted by wetting and non-wetting droplets on suspended and supported monolayer and multilayer graphene samples. ESEM experimental observations on suspended monolayer graphene over a holey substrate atop a TEM grid with closed holes similar to those reported by Zhang et al. were also carried out in our work and can be seen in **Figure S8** in the accompanying Supplementary Note 3. ESEM Experimental Observations. To highlight is the remarkable agreement on the contact angles reported by Zhang et al. [31] and those reported in in the accompanying Supplementary Note 3. ESEM Experimental Observations and **Figure S8** for droplets sitting fully on the suspended graphene droplets resting partially on both suspended and supported graphene with closed holes.

Figure 3 presents direct ESEM experimental observations of condensation on $1L^{sus}$, $2L^{sus}$, $4L^{sus}$, and ML^{sus} with open holes in time. While the accompanying Supplementary Movies 1 to 6 contain the ESEM images of the 6 panels (a-f) presented in **Figure 3** and were captured at approximately 1 frame every 5 seconds highlighting the quasi-steady state of our observations.

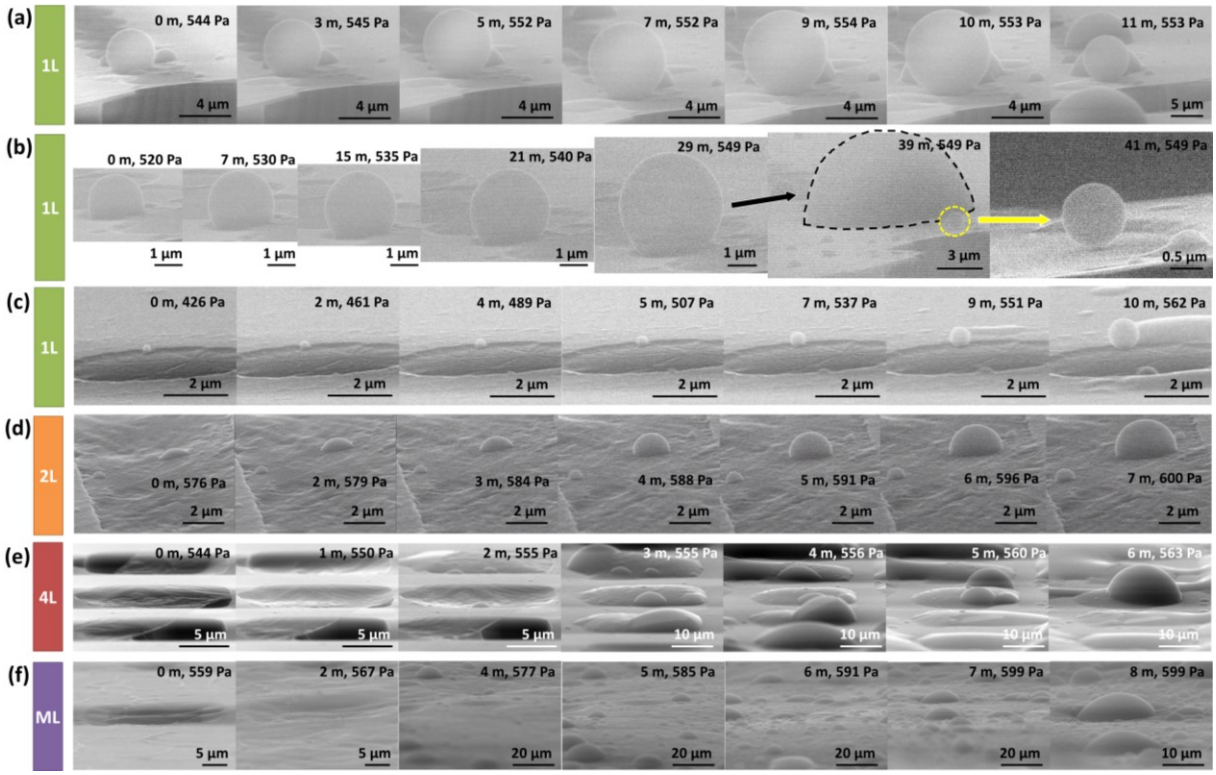

Figure 3 ESEM experimental observations of condensation. (a-c) $1L^{sus}$, **(d)** $2L^{sus}$, **(e)** $4L^{sus}$, and **(f)** ML^{sus} in time (see accompanying **Supplementary Movies 1** to **6**). Non-wetting water droplets are only observed on suspended graphene ($1L^{sus}$). We note here that experimental observations on **(a-b)** and **(c)** correspond to 2 different samples prepared by the same fabrication procedure reported in section 4.1 Sample Fabrication and in the accompanying Supplementary Note 1.Substrate Fabrication. Relative condensation time with respect to the first frame, environmental pressure and scale bars reported from ESEM experimental observations are included for each frame (more details on the ESEM experimental procedure and observations can be found in Section 4.3 ESEM Experimental Observations and within the accompanying Supplementary Note 3. ESEM Experimental Observations).

Figure 3a,b,c show non-wetting droplets growing in a quasi-steady state on $1L^{sus}$ with contact angles approaching 180° before spreading, whereas on $2L^{sus}$, $4L^{sus}$, and ML^{sus} (**Figure 3d,e,f**) droplets grow in a quasi-steady state in the partial wetting regime. As shown in **Figure 3a,b,c**, non-wetting droplets grow from around 110º to 175º with an average contact angle of around 160º. **Figure 3a,b,c** show droplets growing in a quasi-steady state with an increasing contact angle and base diameter until the droplet reaches the supported graphene and then suddenly spreads as in **Figure 3a,b** and **Figure S9(top)** and **Figure S9(middle)** in the accompanying Supplementary Note 3. ESEM Experimental Observations. This growth with both contact angle and base diameter increasing is different from the advancing constant contact angle mode reported during condensation on superhydrophobic surfaces, which is attributed to the absence of nanoscale pinning as well as the quasi-steady growth conditions imposed[15,26]. It is worth noting that during

droplet growth in the quasi-steady state in both cases the base diameter increases with time, though they occur at different rates, which cannot rule out the absence of nanoscale pinning on suspended monolayer graphene, and this latter could be attributed to chemical and/or physical heterogeneities of the surface. In these two cases, the last snapshot/frame before the droplet spreads as a consequence of the advancing droplet contact line reaching the supported graphene region is adopted for the representation of the non-wetting droplet contact angles in **Figure 4** in the main manuscript. Here, we define "non-wetting droplet" as a droplet with a measured contact angle (or advancing contact angle henceforth referred to as contact angle) larger than 120º, which was known to be the hydrophobic limit/barrier for any smooth hydrophobic surface set by Teflon™ [4,11].

Non-wetting droplets were found to be reproducible on the same sample even after five condensation-evaporation cycles. This evidences the differences in wettability between $1L^{sus}$ when compared to $1L_{sup}$. This is further ascertained with the observations of the main droplet in **Figure 3b**, which initially grows in the non-wetting regime while the base of the droplet is on $1L^{sus}$, and as the droplet grows bigger and the triple contact line touches the supported region ($1L_{sup}$) the droplet suddenly spreads, *i.e.*, it transitions from non-wetting on $1L^{sus}$ to partial wetting on $1L_{sup}$. The largest contact angle of a droplet on $1L^{sus}$ approaches 180º as in the right side of **Figure 3b**, which resembles the ideal shape of a free-standing droplet in vacuum and/or in air. To further confirm that the presence of non-wetting droplets with contact angles approaching 180° is solely an inherent property of $1L^{sus}$, **Figure 4** includes independent contact angle measurements on both 1L, 2L, 4L and ML suspended and supported graphene at different condensation intervals. In addition, **Figure 4** shows experimental observations of droplets on 1L, 2L, 4L and ML samples simultaneously on both supported and suspended regions. And provides a direct quantitative comparison between the contact angle measurements for monolayer graphene suspended over closed holes of this work and that of Zhang et al.[31]. The suspended and supported graphene areas are marked in **Figure 4** and they can be clearly distinguished by the position of the edges.

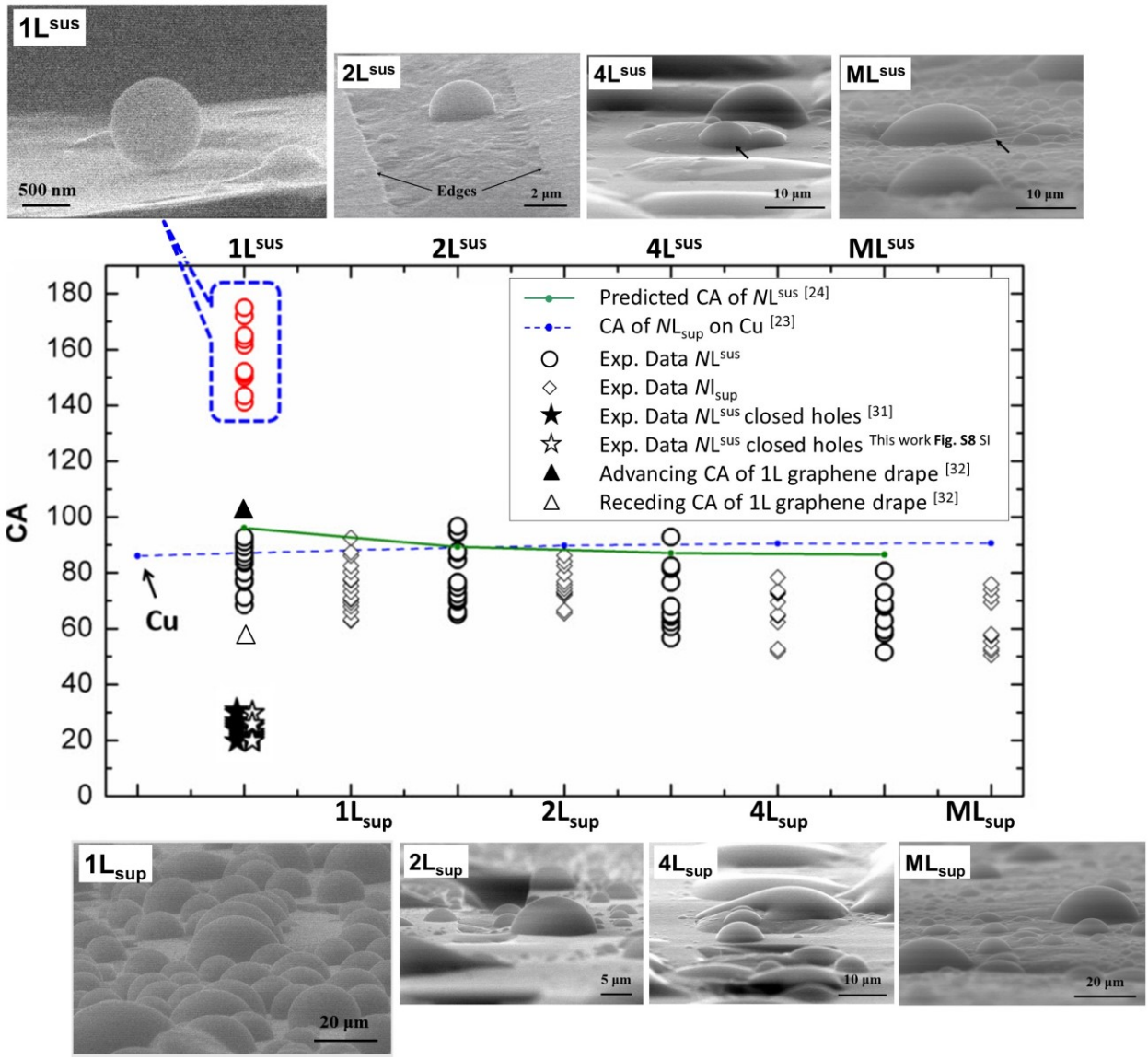

Figure 4 | Wettability on supported and on suspended monolayer and multilayer graphene. (circles) Contact angles, CA or θ (deg), of droplets on suspended: $1L^{sus}$, $2L^{sus}$, $4L^{sus}$, and ML^{sus}, and (diamonds) contact angles of droplets on supported: $1L_{sup}$, $2L_{sup}$, $4L_{sup}$, and ML_{sup} where N refers to the number of layers. For each case, 10 to 20 independent CA measurements are reported. Theoretical CA trend based on the minimum Lennard-Jones (L-J) potential for suspended graphene as in Ref. 24 is plotted as a green solid line , while blue dashed line includes theoretical CA calculation of supported graphene on copper (Cu) from Ref. 23, for comparison. ESEM snapshots of (top) droplets on $1L^{sus}$, $2L^{sus}$, $4L^{sus}$ and ML^{sus} samples, and (bottom) droplets on $1L_{sup}$, $2L_{sup}$, $4L_{sup}$ and ML_{sup} samples are included for comparison. Non-wetting droplets on $1L^{sus}$ are represented as red circles. CA measurements of wetting droplets on suspended monolayer graphene supported over a TEM grid with closed holes from (open stars) our work **Figure S8(b)** in the accompanying Supplementary Note 3. ESEM Experimental Observations and (closed stars) the work of Zhang et al. Ref. 31 are included for comparison. Advancing CA (closed triangles) and receding CA (open triangles) of large-area 1L graphene drape from Ref. 32 are also included (note that the x-axis representation for suspended monolayer graphene with closed holes is slightly shifted so that the two conditions can be readily identified).

Figure 4 shows that droplets on $1L^{sus}$ have contact angles as high as 175º while droplets on $1L_{sup}$ display contact angles close to or below 90º. In the case of 2L, 4L and ML, contact angles of droplets on both suspended and supported samples are practically the same and in the partial wetting regime with values close to 90º or below 90º, which are also similar to those reported here for water droplets on $1L_{sup}$ and consistent with the literature[22]. Non-wetting contact angles on $1L^{sus}$ reported in this work and in **Figure 4** differ from the dynamical contact angles (102º advancing contact angle and 60º receding contact angle) of large-area 1L graphene drape[32,33] and wetting contact angles reported on partially suspended monolayer graphene (solid surface fractions as low as 5%) in the work of Ondarçuhu *et al.*[34]. Non-wetting behaviour reported in this work is mainly due to the complete suppression of any substrate interaction, which is entirely removed from underneath the footprint of the droplets coupled with the presence of an adsorbed layer of water above and below the $1L^{sus}$ as per the high humidity environmental conditions studied under ESEM. Note that spreading of a non-wetting droplet growing on $1L^{sus}$ was observed once the advancing contact line of the non-wetting droplet reached the $1L_{sup}$ as shown in **Figure 3b**. In addition, the agreement between the wettability of suspended monolayer graphene supported over a TEM grid with closed holes reported both in this work (accompanying Supplementary Note 3. ESEM Experimental Observations and **Figure S8**) and that of Zhang et al.[31] is further provided within **Figure 4**. The occurrence of partially wetting droplets reported on $1L^{sus}$ with open holes is attributed to the current inability of the scientific community of fabricating 100% full crystalline, wrinkle free and clean suspended graphene of the sizes required. The presence of amorphous regions, wrinkles and hydrocarbons may induce surface defects which in turn decrease the energy barrier for nucleation favouring condensation on those regions[35,36]. This provides a plausible and reasonable explanation for the occurrence of the bimodal contact angle distribution showing both wetting and non-wetting droplets on the same $1L^{sus}$.

Discussion

Nucleation

In macroscopic wetting studies, to assess the extent of pinning the droplet contact line is advanced or receded by addition or withdraw of liquid to the droplet. In contrast, in the ESEM approach the contact line advances by condensation of molecules and, significantly, can overcome small irregularities on the surface. Although nanoscale defects can induce pinning[37], the quasi-steady droplet growth imposed where condensing molecules build up at the triple phase contact line and at the liquid-gas interface can overcome the pinning energy barrier via thermal fluctuations and/or external forces[38]. Additionally, it is worth noting that condensation shall preferentially take place on such topological or chemical defects; however, based on the Kelvin equation, the cluster size necessary for nucleation is orders of magnitude larger than any of the defects measured on our $1L^{sus}$ reported in **Figure 2b**. To estimate the extent of this we consider the critical droplet radius for nucleation, r_e, by making use of the Kelvin equation $r_e = {2T_v\gamma_{lv}}/{h_{fg}\rho_l\Delta T}$ where T_v is the temperature of the vapor, γ_{lv} is the liquid-vapor interfacial tension, h_{fg} the latent heat of vapor to liquid phase-change, ρ_l the density of the liquid and ΔT the subcooling temperature[36,39]. In the present conditions where ESEM works near the liquid-vapor saturation curve[40], r_e is of the order of tens of nanometers, which is one order of magnitude greater than the smallest sized nucleated droplet observed and two orders of magnitude greater than the average of the defects found in $1L^{sus}$ (see calculations on r_e versus ΔT in the accompanying Supplementary Note 5. Minimum radius for nucleation and **Figure S11**, and AFM characterization of $1L^{sus}$ in **Figure 2b** and in the accompanying Supplementary Note 2.2 AFM Topography Characterization of Surface Roughness of Graphene). This estimation points out that the cluster size of the molecules required for nucleation is orders of magnitude greater than the defects present. This suggests that pinning of the contact line by small defects on the nm scale is unlikely to explain the observation of non-wetting droplets on $1L^{sus}$.

Statistical Analysis

Statistical analysis reported in the accompanying Supplementary Note 4. Statistical Analysis indirectly demonstrates the occurrence of non-wetting droplets with contact angles approaching 180° is unique to suspended monolayer graphene. While at the same time it rules out the occurrence of such non-wetting droplets on supported mono- to multi-layer and suspended double to multi-layer graphene. A total of 0 non-wetting droplets with contact angles approaching 180°

were reported on these substrates from more than 3,200 droplets analysed while the occurrence of non-wetting with contact angles approaching 180° was intrinsic to suspended monolayer graphene with 100% of the occurrences on these five tested samples (samples #1 to #5 in **Figure S7** in the accompanying Supplementary Note 3. ESEM Experimental Observations). While one would expect that the greater contamination, roughness and/or pinning on supported and multilayer graphene provides additional sites for the occurrence of non-wetting, our observations attribute this unique behaviour to suspended monolayer graphene **Figure S7** in the accompanying Supplementary Note 5. Minimum radius for nucleation. Moreover, the simultaneous occurrence of spherical non-wetting and partial wetting droplets on $1L^{sus}$ and $1L_{sup}$, respectively, shown in **Figure 4** within the same frame under the same temperature and pressure conditions provides evidence for unique non-wetting properties of $1L^{sus}$. On other hand, the rather low occurrence of non-wetting droplets with contact angles approaching 180° (10.7% out of 112 droplets analysed) is attributed to other factors such as cleanliness, amorphousness, wrinkles, contamination, etc. Complete statistical data and analysis is shown in the accompanying Supplementary Note 4. Statistical Analysis and **Figure S10**. Unfortunately further insights and considerations on the low occurrence of non-wetting contact angles approaching 180° are not possible with current available graphene fabrication procedures and experimental observation methodologies to date.

Pinning Considerations

Further, nanoscale defects increase in size and number as the number of graphene layers increase; hence if pinning on such defects were to be the reasons for the non-wetting droplets observed, such behaviour should have been reported on the rest of supported and suspended graphene substrates with multiple layers. Despite the greater degree of nanoscopic defects and roughness of $1L_{sup}$, 2L, 4L and ML, when compared to $1L^{sus}$ (see **Figure 2** and in the accompanying Supplementary Note 2.2 AFM Topography Characterization of Surface Roughness of Graphene and **Figure S5** and **S6**), which should promote contact line pinning, the lack of non-wetting droplets on of $1L_{sup}$, 2L, 4L and ML (0 drops out of more than 2000 observations) suggests that surface contamination, roughness and/or pinning may not be the mechanism for the non-wetting behaviour with contact angles approaching 180° reported here on $1L^{sus}$. An intrinsic limitation in these experiments is that because of the small volume of the imaged droplets limited by the $1L^{sus}$ sample size and the quasi-steady ESEM imaging technique utilized, any receding of the triple contact line before complete evaporation cannot be captured.

Theory

Theoretical trends based on the Lennard-Jones (L-J) potential offer a reasonable explanation for the contact angles of wetting droplets reported on multilayer graphene but cannot explain the case of suspended monolayer[24]. Under ESEM operating conditions, the environment is saturated with water vapor and hence the suspended graphene layer is surrounded by water vapor where the polar interactions of water molecules above and below graphene could act across this one atomic layer, as suggested in recent works[23]. Recent ESEM experiment of water condensation on single side of graphene[31] and additional experiments reproducing the conditions reported in Ref. 31 carried out in this investigation so to validate our approach (accompanying Supplementary Note 3. ESEM Experimental Observations and **Figure S8**) indicate that non-wetting droplets can be seen exclusively on suspended monolayers open to the ambient on both sides and not on monolayer graphene where either of the sides is closed to the environment. The present findings may be relevant to further understanding monolayer wettability and offer additional elements on the wetting translucency and the high slippage of graphene upon interaction with water molecules as reported recently[23,41-43].

Additional Considerations

Although experimental observations and statistical analysis shows the occurrence of non-wetting droplets with contact angles approaching 180° on suspended monolayer graphene before drawing the conclusion, we would like to summarise the limitations of the methodology used in this study. Although the experimental technique adopted permits a dynamic observation (1 frame every 4 or 5 seconds) with a rather good spatial resolution (from few tens of pixels per micrometre to hundreds of pixels per micrometre), we acknowledge that the large tilting angle coupled with the opaqueness of water to the ESEM electron beam and to the simultaneous occurrence of condensation over the substrate may hinder the accurate measurement or influence to some extent the wettability and contact angle measurements reported here. Nonetheless, although there may be some differences in the contact angles reported, distinction between non-wetting (contact angles approaching 180°) and wetting is perfectly identifiable from the observations. We also note here that the different dynamics of the advancing motion of the contact line are attributed to the slow droplet growth in the quasi-steady regime, so to allow imaging, and/or to the presence of chemical and/or physical heterogeneities on the surface, which cannot be quantified with current available characterisation techniques. As well as we would have expected the occurrence of non-wetting droplets on other fabricated substrates if pinning alone were to be the sole reason for the

observations reported. On the other hand, the statistical analysis proposed has been limited to the number of experimental observations and substrates used. Although the number of observation could be increased which can influence the percentage of non-wetting occurrences with contact angles approaching 180° on suspended monolayer graphene, a single non-wetting occurrence does support the unique behaviour when compared to the other studied samples. While the adsorption of water molecules on both sides of the suspended graphene monolayer represents a plausible mechanism, we expect other reasonable arguments or mechanisms may follow so to further complement the proposed one to account for the observations reported. Last, although our graphene samples were prepared following traditional Chemical Vapour Deposition (CVD) methods reported in the literature and local measurements of both Raman, AFM, TEM and Electron Diffraction (ED) patterns suggests on the cleanliness and high quality of the studied sample, we acknowledge that such local measurements do not ensure the high quality of the suspended and supported graphene over the large fabricated areas.

Conclusions

Direct experimental observations of micrometer/picoliter droplets condensing on monolayer suspended graphene are used to characterize its inherent wettability. The observation of non-wetting droplets with contact angles as high as 175° are reported exclusively on a smooth atomically flat monolayer suspended graphene, whereas wetting droplets with contact angles below 90° are reported on supported monolayer and on supported and suspended multiple layers graphene. Experimental observations demonstrate that non-wetting of water droplets on smooth monolayer may be possible by removing the water-surface interactions beyond the first surface layer in the case of graphene. As water vapour molecules condense, these form an ordered layer at both sides of the suspended graphene interacting with each other first. Then further condensing water molecules become shielded from the interactions with the graphene and spherical droplets ensue so to minimise surface energy. This suggests the maximum contact angle attainable on a smooth hydrophobic surface may not be limited to that of Teflon™.

The present observations open the door to wettability manipulation through suspended graphene. This could be achieved through control of the environment behind the suspended graphene layer such as the use of microfluidics and calls for the further investigations on other monolayer materials.

Methods

Substrate fabrication

The fabrication procedure was as follows: monolayer graphene was grown on copper foil by using standard Chemical Vapor Deposition (CVD) method[44]. Then, the graphene was transferred onto a SiO_2/Si target substrate by using common poly(methyl-methacrylate) (PMMA) transfer method. To create well defined holes and trenches, prior to the graphene transfer procedure, the SiO_2/Si target substrate was subjected to Electron Beam (EB) lithography and reactive ion etching (RIE). After the transfer procedure and in order remove the PMMA layer, the SiO_2/Si target sample coated with graphene and PMMA was dipped into acetone at ~50 °C for more than 4 hours. The warmth of the solvent as well as the sufficient immersion time induced the thorough PMMA removal and minimizes contamination and residual PMMA left on the graphene[44,45]. To avoid the rupture of the membrane, the final step consisted on drying the graphene sample by using an HITACHI HCP-2 supercritical point dryer. The high quality of the suspended graphene sample was confirmed by Scanning Electron Microscopy (SEM), Atomic Force Microscopy (AFM), Tunneling Electron Microscopy (TEM) and Raman spectroscopy (see Fig. 2 in the main text). In addition to monolayer graphene (1L), double-layer graphene (2L) and four-layer (4L) samples were prepared by stacking the monolayer graphene several times following the same CVD growth and the same PMMA transfer procedures reported above[45]. On the other hand, multi-layer graphite (ML) sample was prepared by mechanical exfoliation method and then transferred onto the substrate.

Sample Characterization

Within the accompanying Supplementary Information, we follow the same nomenclature as established within the main text. We do henceforth refer to suspended graphene with the superscript ^{sus} and to supported graphene with subscript $_{sup}$. From the surface characterization by optical microscopy and SEM shown in Fig. 2a (main text), the successful fabrication of both $1L^{sus}$ and $1L_{sup}$ is demonstrated. 1L graphene was completely suspended ($1L^{sus}$) over holes with up to 5 μm in diameter and over trenches of 5 μm in width and tens of micrometers in length. From Fig. 2a (main text), we note the optical transparency of graphene to SEM as previously reported[46]. When looking into AFM topography characterization, Fig. 2b (main text) shows that the roughness of $1L^{sus}$ is slightly smaller than that of $1L_{sup}$ on the smooth substrate. The latter indicates that the suspended graphene membrane is quite smooth and most of the polymer residues have been removed from the surface. In addition, the lower-right inset of Fig. 2c (main text) presents a high-

resolution TEM image of $1L^{sus}$ showing the clean lattice with perfect honeycomb structure, which is characteristic of high quality graphene. From Fig. 2c (main text), some nanoscale islands of residues can be perceived on the graphene, which may serve as nuclei for the condensation experiment. In addition, ED pattern (top-right inset in Fig. 2c (main text)) exhibits the perfect 6-fold symmetry of the carbon atoms, which is also characteristic of high quality graphene. Finally, Fig. 2d (main text) shows Raman spectra of 1L, 2L, 4L and ML. For 1L, the height of the 2D peak (~2700 cm^{-1}) is almost twice as large as that of the G peak (~1580 cm^{-1}) evidencing the monolayer structure[46]. The height ratio between 2D and G peaks decreases as the number of graphene layers increase. For ML sample, the 2D peak is much wider and shorter than the G peak, which is consistent with literature. It is worth noting that the D peak (~1300 cm^{-1}) is almost absent for all four samples, which highlights the negligible defects of the carbon lattice. Next, we include additional optical microscopy, SEM and AFM topography characterization of 1L, 2L, 4L and ML graphene fabricated substrates. More details on the Sample Characterisation can be found in Supplementary Note 2. Sample Characterisation of 1L Suspended Graphene.

ESEM Experimental Observations

Experimental observations of condensation were undertaken in an Environmental Scanning Electron Microscope (ESEM) FEI Versa 3D™ (Hillsboro, Oregon, U.S.A.), where temperature of the surface and the vapor pressure of the environment could be finely controlled. Graphene sample was fixed to a 45° sample holder using double side carbon tape and then the sample holder was fixed onto the Peltier stage also making use of double side carbon tape at the bottom of the holder, to allow for experimental observations at a tilting angle of ca. 80° with respect to the electron beam. Owed to the additional heat transfer resistances from the Peltier stage to the graphene samples, i.e., two layers of double side carbon tape and the sample holder, the initial temperature of the Peltier stage was set to -1 ºC on the graphene surface, so to ensure a substrate temperature of near 0 ºC, which was further confirmed by additional measurements with an external thermocouple. Once the graphene sample was placed on the Peltier stage, the chamber was vacuumed for several minutes to ~10^{-3} Pa, removing any presence of non-condensable gases, and thereafter the chamber was set into Environmental Scanning Electron Microscopy (ESEM) mode. Then, the vapor pressure was slowly increased at an approximate rate of 20 Pa/min from ~100 Pa until the first nucleated droplets were observed. The pressure rate was increased at the lowest rate of 6 Pa/min and/or manually in increment steps of 1 Pa ensuing the condensate growth in a quasi-steady state.

As system pressure is increased the relative humidity, i.e., amount of vapor water molecules in the environment, accordingly increases following the liquid-vapor equilibrium saturation curve. Nonetheless, changes in the system pressure and hence in the humidity were constrained within 1% per minute so to minimise dynamic effects and disjoining pressure differences during the observations. The temperature of the Peltier stage and the water vapour pressure were precisely controlled with the xT Microscope Control software with an average deviation from the liquid-vapour equilibrium saturation curve of ± 0.3 ºC and ± 16 Pa and a maximum deviation of ± 0.7 ºC and ± 30 Pa [40], while the relative humidity content was above 95%. We note here that experimental observations were carried out at an overall tilting angle of 80° with respect to the electron beam, which should in turn introduce an error in the height of the droplet of less than 2%, i.e., $\cos 0° - \cos 10° = 0.015$, and hence negligible effect on the contact angles reported.

The dynamics of droplet growth was recorded by the software at 1 frame every ca. 3 seconds. After each experimental observation, in order to evaporate the water condensed, the vapor pressure was decreased at low rates to avoid the rupture of graphene. More details on the Sample Characterisation via ESEM experimental observations can be found in SI-3. ESEM Experimental Observations in the accompanying Supplementary Information.

Data Availability

Supplementary Information is available from the Communication Materials online article or from the authors, while all the data that support the findings of this study or any other datasheets or data generated during the current study are available from the first and second authors as well as from the corresponding author upon reasonable request.

Correspondence and requests for materials should be addressed to K.S. ksefiane@ed.ac.uk

Acknowledgements

H.W acknowledges the support of the National Youth 1000 Talents Program in China with Nos. 51976096, while H.W. and X.Z. acknowledge the support of the National Natural Science Foundation of China Grant Nos. 51827807. K.S. and D.O. acknowledge the support received from the European Space Agency (ESA) under the project Convection and Interfacial Mass Exchange (EVAPORATION) with ESA Contract Number 4000129506/20/NL/PG. D.O. acknowledges the support received from JSPS KAKENHI Early Career Scientists with Grant No. JP18K13073. D.O. and Y.T. acknowledge the support receive from the International Institute for Carbon-Neutral Energy Research (WPI-I2CNER), sponsored by the Japanese Ministry of Education, Culture, Sports, Science and Technology MEXT.

Author Contributions

K.S. conceived the idea, K.S., H.W. and D.O. developed the methodology; K.S., G.M., H.W. and D.O. carried out the investigation and analysis; H.W. and D.O. carried out the experimental observations and visualisation; K.S., Y.T., H.T., X.Z. and H.W. contributed with funding acquisition; K.S., was in charge of project administration; the project was supervised by K.S., Y.T., H.T. and X.Z; the original draft was completed by K.S., G.M., H.W. and D.O.; and all the authors H.W., D.O., D.S., X.Z., G.M., H.T., Y.T. and K.S..

Competing Interests Statement

The authors declare no conflict of interest, competing or financial interests associated to this publication.

Supplementary Information

Figures' Captions

Figure 1 | Schematic representation of wetting and non-wetting of liquids on various materials. (a) non-wetting on bulk rigid Teflon™ and on surface coated with a thin film of Teflon™, **(b)** non-wetting on superhydrophobic structured Teflon™ bed of nails, **(c)** non-wetting on a very hot rigid material, **(d)** wetting of hydrophobic Teflon™ thin film wrapping itself around the droplet as in Capillary Origami[20], **(e)** wetting on suspended and on supported multilayer graphene, and **(f)** wetting on supported monolayer graphene and non-wetting on suspended monolayer graphene where non-wetting droplet is highlighted by a red dashed circle.

Figure 2 | Surface characterization of 1L graphene. (a) Scanning Electron Microscopy (SEM), **(b)** Atomic Force Microscopy (AFM) height image of an area of 7.5×7.5 μm^2, **(c)** Tunnelling Electron Microscopy (TEM) and **(d)** Raman spectroscopy. Figure 2b also includes the root mean square surface roughness of suspended monolayer graphene, R_a^{sus} = 0.4 nm. Inset of Figure 2c bottom-right includes enlarged high-resolution TEM image and top-right shows Electron Diffraction (ED) pattern of $1L^{sus}$. Figure 2d shows Raman spectra of 1L, 2L, 4L graphene and ML graphite, where the intensity ratio between 2D band (~2700 cm^{-1}) and G band (~1580 cm^{-1}) correlates to number of layers with an I2D/IG ratio of nearly 5 for $1L^{sus}$ in agreement with Ref. 34.

Figure 3 | ESEM experimental observations of condensation. (a-c) $1L^{sus}$, (d) $2L^{sus}$, **(e)** $4L^{sus}$, and **(f)** ML^{sus} in time (see accompanying Supplementary Information **Supplementary Movies S1** to **S6**). Non-wetting water droplets are only observed on suspended graphene ($1L^{sus}$). We note here that experimental observations on **(a-b)** and **(c)** correspond to 2 different samples prepared by the same fabrication procedure reported in section 4.1 Sample Fabrication and in the accompanying Supplementary Information SI-1.Substrate Fabrication. Relative condensation time with respect to the first frame, environmental pressure and scale bars reported from ESEM experimental observations are included for each frame (more details on the ESEM experimental procedure and observations can be found in Section 4.3 ESEM Experimental Observations and within the accompanying Supplementary Information SI-3. ESEM Experimental Observations).

Figure 4 | Wettability on supported and on suspended monolayer and multilayer graphene. (circles) Contact angles, CA or θ (deg), of droplets on suspended: $1L^{sus}$, $2L^{sus}$, $4L^{sus}$, and ML^{sus}, and (diamonds) contact angles of droplets on supported: $1L_{sup}$, $2L_{sup}$, $4L_{sup}$, and ML_{sup}, where N refers to the number of layers. For each case, 10 to 20 independent CA measurements are reported. Theoretical CA trend based on the minimum Lennard-Jones (L-J) potential for suspended graphene as in Ref. 24 is plotted as a green solid line , while blue dashed line includes theoretical CA calculation of supported graphene on copper (Cu) from Ref. 23, for comparison. ESEM snapshots of (top) droplets on $1L^{sus}$, $2L^{sus}$, $4L^{sus}$ and ML^{sus} samples, and (bottom) droplets on $1L_{sup}$, $2L_{sup}$, $4L_{sup}$ and ML_{sup} samples are included for comparison. Non-wetting droplets on $1L^{sus}$ are represented as red circles. CA measurements of wetting droplets on suspended monolayer graphene supported over a TEM grid with closed holes from (open stars) our work **Figure S8(b)**

in the accompanying Supplementary Information SI-3. ESEM Experimental Observations and (closed stars) the work of Zhang et al. Ref. 31 are included for comparison. Advancing CA (closed triangles) and receding CA (open triangles) of large-area 1L graphene drape from Ref. 32 are also included (note that the x-axis representation for suspended monolayer graphene with closed holes is slightly shifted so that the two conditions can be readily identified).

References

1. Nishimoto, S. & Bhushan, B. Bioinspired self-cleaning surfaces with superhydrophobicity, superoleophobicity, and superhydrophilicity. *RSC Adv.* **3**, 671-690 (2013).
2. Kirschner, C. M. & Brennan, A. Bio-inspired antifouling strategies. *Annu. Rev. Mater. Res.* **42**, 211-219 (2012).
3. Yao, X., Song, Y. & Jiang, L. Applications of bio-inspired special wettable surfaces, *Adv. Matter.* **23**, 719-734 (2011).
4. Adamson, A. W. & Gast, A. P. *Physical Chemistry of Surfaces* (Wiley-Blackwell, 1997).
5. Barthlott, W. & Neinhuis, C. Purity of the sacred lotus, or escape from contamination in biological surfaces. *Planta* **202**, 1-8 (1997).
6. Neinhuis, C. & Barthlott, W. Characterization and distribution of water-repellent self-cleaning plant surfaces. *Ann. Bot.* **79**, 667-677 (1997).
7. Onda, T., Shibuichi, S., Satoh, N. & Tsujii, K. Super-water-repellent fractal surfaces. *Langmuir* **12**, 2125-2127 (1996).
8. Lafuma, A. & Quéré, D. Superhydrophobic states. *Nat. Mater.* **2**, 457-460 (2003).
9. Wang, S. & Jiang, L. Definition of Superhydrophobic States. *Adv. Mater.* **19**, 3423-3424 (2007).
10. Leidenfrost, J. G. *De aquae communis nonnullis qualitatibus tractatus* (Duisburgh 1756).
11. Biance, A. -L., Clanet, C. & Quéré, D. Leidenfrost drops. *Phys. Fluids* **15**, 1632-1637 (2003).
12. Öner, D. & McCarthy, T. J. Ultrahydrophobic surfaces. Effects of topography length scales on wettability. *Langmuir* **16**, 7777-7782 (2000).
13. Tuteja, A., Choi, W., Ma, M., Mabry, J. M., Mazzella, S. A., Rutledge, G. C., McKinley, G. H. & Cohen, R. E. Designing superoleophobic surfaces. *Science* **318**, 1618-1622 (2007).
14. Liu, T. "Leo" & Kim, C. -J. "CJ". Turning a surface superrepellent even to completely wetting liquids. *Science* **346**, 1096-1100 (2014).
15. Yan, X. et al. Atmosphere-mediated superhydrophobicity of rationally designed micro/nanostructured surfaces. *ACS Nano* **13**, 4160-4173 (2019).
16. Quéré, D. Wetting and roughness. *Annu. Rev. Mater. Res.* **38**, 71-99 (2008).
17. Saran, R., Fox, D., Zhai, L. & Chanda, D., Organic Non-Wettable Superhydrophobic Fullerite

Films, *Adv. Mater.* **33**, 2102108 (2021).

18. Schutzius, T. M., Jung, S., Maitra, T., Graeber, G., Köhme, M. & Poulikakos, D. Spontaneous droplet trampolining on rigid superhydrophobic surfaces. *Nature* **527**, 82-85, 2015.
19. Celestini, F., Frisch, T. & Pomeau, Y. Room temperature water Leidenfrost droplets. *Soft Matter* **9**, 9535-9538, 2013.
20. Py, C., Reverdy, P., Doppler, L., Bico, J., Roman, B. & Baroud, C. Capillary Origami: Spontaneous wrapping of a droplet with an elastic sheet. *Phys. Rev. Lett.* **98**, 2-5 (2007).
21. Gao, L. & McCarthy, T. J. Teflon is hydrophilic. Comments on definitions of hydrophobic, shear versus tensile hydrophobicity and wettability characterization. *Langmuir* **24**, 9183-9188 (2008).
22. McHale, G. All solids, including Teflon, are hydrophilic (to some extent), but some have roughness induced hydrophobic tendencies. *Langmuir* **25**, 7185-7187 (2009).
23. Rafiee, J., Mi, X., Gullapalli, H., Thomas, A. V., Yavari, F., Shi, Y., Ajayan, P. M. & Koratkar, N. A. Wetting transparency of graphene. *Nat. Mater.* **11**, 217-222 (2012).
24. Shih, C. -J., Want, Q. -H., Lin, S., Park, K. –C., Jin, Z., Strano, M. S. & Bankschtein, D. Breakdown in the wetting transparency of graphene. *Phys. Rev. Lett.* **109**, 176101 (2012).
25. Shih, C. -J., Want, Q. -H., Lin, S., Park, K. –C., Jin, Z., Strano, M. S. & Bankschtein, D. Erratum: Breakdown in the wetting transparency of graphene [Phys. Rev. Lett. **109**, 176101 (2012)]. *Phys. Rev. Lett.* **115**, 49901 (2015).
26. Yan, X. et al. Droplet jumping: effects of droplet size, surface structure, pinning, and liquid properties. *ACS Nano* **19**, 1309-1323 (2019).
27. Prydatko, A. V., Belyaeva, L. A., Jiang, L., Lima, L. M. C. & Scheider, G. F. Contact angle measurement of free-standing square-millimeter single-layer graphene. *Nature Commun*. **9**, 4185 (2018).
28. Bera, B., Shahidzadeh, N., Mishra, H., Belyaeva, L. A., Schneider, G. F. & Bonn, D. Wetting of water on graphene nanopowders of different thicknesses. *Appl. Phys. Lett.* **112**, 151606 (2018).
29. Chang, W., Peng, B. L., Khan, A. S., et al. Grain size effects on the wettability of as-grown graphene and dropwise condensation. *Carbon* **171**, 507-513 (2021).
30. Raj, R., Maroo, S. C., Wang E. N. Wettability of graphene. *Nano Lett.* **13**, 1509-1515 (2013).
31. Zhang et al. Intrinsic Wettability in Pristine Graphene. *Adv. Mater.* 34 (6), 2103620 (2021).
32. Singh, E., Thomas, A. V., Mukherjee, R., et al. Graphene drape minimizes the pinning and hysteresis of water drops on nanotextured rough surfaces. *ACS Nano* **7**, 3512-3521 (2013).

33. Ghoshal, D., Jain, R., Koratkar, N. Graphene's partial transparency to van der Waals and electrostatic interactions. *Langmuir* **35**, 12306-12316 (2019).
34. Ondarçuhu, T., Thomas, V., Nuñez, M., Dujardin, E., Rahman, A., Black, C. T. & Checco, A. Wettability of partially suspended graphene. *Sci Rep* 6, 24237 (2016).
35. Li, Z., et al. Effect of airborne contaminants on the wettability of supported graphene and graphite. *Nature Materials* **12**, 925-931 (2013).
36. Fisher, L. R. & Israelachvili, J.N. Direct experimental verification of the Kelvin equation for capillary condensation *Nature* **277**, 548-549 (1979).
37. Wang, Y. J., Guo, S., Chen, H.- Y. & Tong, P. Understanding contact angle hysteresis on an ambient solid surface, *Phys. Rev. E* **93**, 052802 (2016).
38. Giacomello, A., Schimmele, L. & Dietrich S. Wetting hysteresis induced by nanodefects. *Proceedings of the National Academy of Sciences* **113** (3) E262-E271 (2016).
39. Maa, J. R., Droplet Size Distribution and Heat Flux of Dropwise Condensation, *The Chemical Engineering Journal* **16**, 171-176 (1978).
40. Orejon, D., Shardt, O., Waghmare, P. R., Kumar Gunda, N. S., Takata, Y. & Mitra, S. K., Droplet migration during condensation on chemically patterned micropillars, *RSC Adv.* **6**, 36698-36704 (2016).
41. Kim, G. -T., Gim, S. -J., Cho, S. -M., Koratkar, N. & Oh, I. -K. Wetting-transparent graphene films for hydrophobic water-harvesting surfaces. *Advanced Materials* **26**, 5166-5172 (2014).
42. Tocci, G., Joly, L. & Michaelides, A. Friction of water on graphene and hexagonal boron nitride from *Ab Initio* methods: very different slippage despite very similar interface structures. *Nano Lett.* **14**, 6872-6877 (2014).
43. Secchi, E., Marbach, S., Niguès, A., Stein, D., Siria, A. & Bocquet, L. Massive radius-dependent flow slippage in carbon nanotubes. *Nature* **537**, 210-213 (2016).
44. Srivastava, A., Galande, C., Ci, L., Song, L., Rai, C., Jariwala, D., Felly, K. F. & Ajayan, P. M. Novel liquid precursor-based facile synthesis of large-area continuous, single, and few-layer graphene films. *Chem. Mater.* **22,** 3457–3461 (2010).
45. Lin, Y.-C., Jin, C., Lee, J.-C., Jen, S.-F., Suenaga, K. & Chiu, P.-W. Clean transfer of graphene for isolation and suspension. *ACS Nano* **5,** 2362–2368 (2011).
46. Nair, R. R., Blake, P, Grigorenko, A. N., Novoselov, K. S., Booth, T. J., Stauber, T., Peres, N. M. R. & Geim A. K. Fine structure constant defines visual transparency of graphene. *Science* **320,** 1308–1308 (2008).